Comparative investigation of electronic transport across three-dimensional nanojunctions

Yun-Peng Wang, X.-G. Zhang, J. N. Fry, and Hai-Ping Cheng

Phys. Rev. B **95**, 085303 — Published 7 February 2017

DOI: 10.1103/PhysRevB.95.085303

A comparative investigation of electronic transport across three-dimensional nano-junctions

Yun-Peng Wang,[1,2] X.-G. Zhang,[1,2] J. N. Fry,[1] and Hai-Ping Cheng[1,2*]
[1] *Department of Physics, University of Florida, Gainesville, Florida 32611, USA*
[2] *Quantum Theory Project, University of Florida, Gainesville, Florida 32611, USA*

We show the thickness dependent transition from metallic conduction to tunneling in three-dimensional (3D) Ag/Si/Ag nano-junctions through layer-by-layer electronic structure and quantum transport calculations. The transmission coefficients are calculated quantum mechanically within the framework of density functional theory in conjunction with non-equilibrium Green's function techniques. Thin junctions show nearly metallic character with no energy gap opening in Si layers due to the metal-induced interface states, and the transmission is independent of the stacking order of Si layers. Energy gap reemerges for Si layers deeply buried within thick junction, and the decay rate of transmission in this insulating region depends on the stacking order. Complex band analysis indicates that the decay of transmission is not determined by a single exponential constant but also depends on the available number of evanescent states. Calculating the electric resistance from the transmission coefficient requires a 3D generalization of the Landauer formula, which is not unique. We examine two approaches, the Landauer-Büttiker formula, with and without subtraction of the Sharvin resistance, and a semi-classical Boltzmann equation with boundary conditions defined by the transmission coefficients at the junction. We identify an empirical upper limit of ~ 0.05 per channel in the transmission coefficient, below which the Landauer-Büttiker formula without the Sharvin resistance correction remains a good approximation. In the high transmission limit, the Landauer-Büttiker formula with Sharvin correction and the semi-classical Boltzmann method reach fair agreement.

I. INTRODUCTION

Currently there is a growing interest in multilayer silicene.[1–7] Simple silicene is a single atomic layer of Si atoms arranged in a two-dimensional buckled honeycomb lattice. Although it was predicted decades ago that free-standing silicene exhibits a massless relativistic behavior near the Fermi energy,[8–11] it was not until very recently that silicene was synthesized on the surfaces of a few metallic substrates.[12–15] Linear electronic dispersions were observed in the silicene/Ag(111) system and were attributed as the signature of Dirac fermions in silicene,[12,13] but subsequent experimental and theoretical studies revealed the absence of Dirac fermions near the Fermi energy. Instead, the electronic structure changes substantially, and the observed linear electronic dispersions are *sp*-bands of Ag or hybrid interface states.[16–21] The atomic structure of multilayer-silicene has not yet been identified experimentally. The surface morphology of multilayer-silicene on Ag(111) has been examined using scanning tunneling microscopy (STM) and scanning electron microscopy (SEM). Growth of the first silicene layer on an Ag(111) substrate forms a 4×4 super cell with respect to the Ag(111) surface and 3×3 with respect to free-standing silicene. For multilayer silicene, a $(\sqrt{3} \times \sqrt{3})$R30° reconstruction with respect to the free-standing silicene has been observed.[1–7] The reconstruction in multilayer-silicene/Ag(111) was reproduced theoretically, and it was predicted that only the surface silicene layer reconstructs.[6]

The current-in-plane (CIP) configuration would seem a natural choice to measure the resistance of silicenes, but the current tends to pass through the highly conducting Ag(111) substrates, which makes measurements of the CIP resistance difficult.[2] Moreover, multilayer silicene grows in the so-called Stranski-Krastanov mode (also known as the layer-plus-island mode), in which[1,2] the first silicene layer forms a continuous film on Ag(111), while subsequent Si atoms form islands of multilayer-silicene. As a result, it is difficult to directly associate the measured CIP resistance with the thickness of a multilayer silicene. It is much easier to perform a current-perpendicular-to-plane (CPP) measurement by placing a conducting probe on top of a multilayer-silicene island and measuring the resistance between the probe and the Ag substrate.

CPP transport in stacked heterostructures is an important research subject in its own right. Stacked heterostructures constructed from dissimilar 2D materials exhibit atomic-scale sharp interfaces due to the weak van der Waals inter-layer interactions. The sharp interfaces along the out-of-plane direction allow band structure engineering of CPP transport properties, for instance, Ref. 22 reports a Dirac semimetal based transistor with a vertical heterostructure. Electronic and optoelectric devices utilizing CPP transport benefit from the ultra-short conducting channels; the length of conducting channels is on the order of layer thickness of 2D materials. Examples of CPP devices include graphene-based vertical transistors[23,24] and photo-detectors[25,26], interlayer tunneling transistors[27] and *p*-*n* vertical junctions[28].

A previous work[29] showed that the nearly metallic transport properties of ultrathin (one and two atomic-layer thick) silicene-based junctions is the result of the metal-induced interface states in the Si spacer, similar to the metal induced gap states in thick semiconductor

junctions[30,31]. The calculated junction resistance is on the same order of magnitude as those of grain boundaries in noble metals[32]. As the Si layer becomes thicker, one expects that the electronic transport will turn into quantum tunneling as these midgap metallic states become evanescent. The question remains whether such a transition from metallic to insulating behavior occurs over atomic distances, or whether it requires the formation of a Schottky barrier, which is usually macroscopic in spatial extent.

Another question raised in the previous work[29] that was not fully addressed is that of the contact resistance in the Landauer-Büttiker formula, which must be corrected for junctions with thin barriers. For 3D systems the correction for the contact resistance is not unique[33–37]. One of the acceptable solutions is to use the semiclassical Boltzmann theory to subtract this contact resistance. For junctions with thick barriers, when the transmission is below a critical value, the contact resistance is negligible with respect to junction resistance and the Landauer-Büttiker formula does not need any correction. This critical transmission value has not been investigated in the past.

The aim of this work is threefold. First, we calculate the transport properties and the electric resistance of Ag/Si/Ag 3D nano-junctions with one to eight atomic layers of Si. Second, we compare two recipes for calculating the electric resistance of 3D nano-junctions, the Landauer-Büttiker formula with Sharvin correction and a multi-scale semiclassical-quantum approach following the semiclassical Boltzmann equation in the relaxation-time approximation. We will find a threshold value for the transmission below which the multichannel Landauer-Büttiker formula does not need a correction. Third, we present a numerical method for solving the semiclassical Boltzmann equation, which has not received much attention since its introduction in Refs. 38 and 39. We also investigate Ni/*h*-BN/Ni junction to provide a comparison between a semiconductor and a strong insulator. Although not the focus of this study, *h*-BN is itself interesting as a stand-alone system because of its layered structure.

The rest of the paper is organized as follows: Computational details are presented in Section II. The calculated results for Ag(111)/multilayer-silicene/Ag junctions are shown in Section III, including details of transmission probabilities and resistances. Complementary calculations on multilayer *h*-BN-based junctions are presented in Sec. IV. Section V contains a final summary. A numerical method for solving the semiclassical Boltzmann equation appears as an Appendix.

II. COMPUTATIONAL METHOD

The atomic model for Ag(111)/multilayer-silicene/Ag(111) junctions was built following the first-principles simulations of bilayer-silicene/Ag(111) interfaces presented in Ref. 6 without considering atomic reconstructions at the interfaces. Structures of junctions with two to eight silicene layers were optimized using the projector-augmented wave[40,41] (PAW) based density functional theory (DFT) as implemented in the Vienna *ab initio* simulation package VASP.[42,43] In this work we employed the generalized gradient approximation (GGA) with the Perdew-Burke-Ernzerhof (PBE) parametrization[44]. The lattice constant of free-standing monolayer-silicene is approximately 4/3 times of the Ag(111) surface, and a supercell consisting of 4×4 Ag(111) layers and 3×3 multilayer-silicene primitive unit cells in the *x*-*y* plane was used to simulate these junctions.[19,29] The lattice constant in the *x*-*y* plane was fixed to that of Ag(111), calculated using the PBE functional to be 2.952 Å; and the lattice constant of multilayer-silicene was $2.952\,\text{Å} \times 4/3 = 3.936\,\text{Å}$. The supercells used in the structural optimization consist of the multilayer silicene and five Ag(111) atomic layers with Ag atoms in the central atomic layer fixed in their bulk positions. During structure optimization, the height of the supercell (along the *z*-direction) and the coordinates of atoms were fully relaxed, until the forces on unfixed atoms were smaller than 0.01 eV/Å.

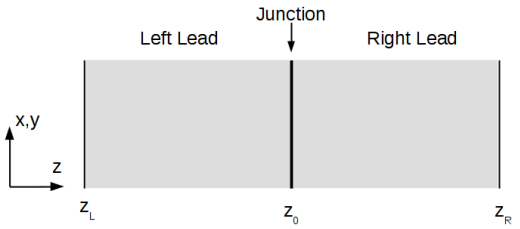

FIG. 1. (Color online) Schematics of a system that consists of n metallic leads separated by $n-1$ junctions in the current-perpendicular-to-plane (CPP) configuration. The electrical current flows in the z direction, and the system is homogeneous in the *x*-*y* plane. In our calculations on multilayer silicene and *h*-BN-based junctions there are two leads and one junction, $n = 2$.

The electrode for *h*-BN junctions is chosen to be *fcc*-Ni because of the small lattice mismatch, 2.504 Å for *h*-BN versus 2.492 Å for the (111)-surface of Ni. The in-plane lattice constant of *h*-BN is squeezed slightly to match that of Ni(111), in order to simulate a commensurate *h*-BN/Ni(111) interface. The distance between *h*-BN layers is set to the interlayer distance in bulk *h*-BN, 3.33 Å. At the *h*-BN/Ni(111) interface, N atoms sit on the top of surface Ni atoms, and the distance between *h*-BN and Ni(111) surfaces is 2.1 Å.[45]

The DFT-based non-equilibrium Green's function[46–48] (NEGF) method was then used to compute the Green's function and the total transmission of these junctions. NEGF calculations were performed using the TRANSIESTA code.[49] Numerical atomic orbitals were used to expand the Hamiltonian and the Green's function. Single-zeta plus polarization (SZP) and double-zeta plus po-

larization (DZP) orbital basis sets for Ag and Si respectively were generated using the default parameters in SIESTA.[50] Norm-conserving pseudopotentials[51] were used to describe interactions between valence electrons ($3s^2 3p^2$ for Si and $4d^{10}5s^1$ for Ag) and the corresponding core electrons. The direction of transport was taken to be the z-direction. Translational symmetry in the x-y plane was exploited by using a 15×15 k-point mesh for calculating the charge density and 55×55 for the Green's function.

The group velocities of Bloch waves in the leads and the transmission and reflection coefficients extracted from first-principles calculations were used as parameters for the Boltzmann equation. The group velocity of the Bloch states within the Ag(111) leads along the z-direction is[29]

$$v_z^j(\mathbf{k}_\parallel) = \frac{a_z}{\hbar}\left[u^j(\mathbf{k}_\parallel)\right]^\dagger \Gamma^{\text{lead}} u^j(\mathbf{k}_\parallel), \tag{1}$$

where a_z is the length of the unit cell of the Ag lead; $u^j(\mathbf{k}_\parallel)$ is the periodic part of the Bloch waves; $\mathbf{k}_\parallel$ are the components of the wavevector in the x-y plane; j is the index for Bloch waves at the same $\mathbf{k}_\parallel$; and $\Gamma^{\text{lead}} = i(\Sigma^r - \Sigma^a)$, where Σ^r and Σ^a are the retarded and advanced self-energies of a Ag unit cell due to coupling with semi-infinite Ag leads. The imaginary part of the self-energy, Γ^{lead}, is equal to the difference in the inverse of the retarded and advanced Green's functions of an isolated Ag unit cell and a Ag unit cell embedded in the bulk. The transmission t and reflection r coefficients corresponding to the Bloch waves in the left and the right leads are[29]

$$t_{j,j'}^{M,N} = \frac{i}{\hbar\sqrt{|v_{z,<}^{M,j}|\,|v_{z,>}^{N,j'}|}}\left(u_>^{N,j'}\right)^\dagger \Gamma_N^{\text{lead}} G_{NM}^r \Gamma_M^{\text{lead}}(u_<^{M,j}), \tag{2}$$

$$r_{j,j'}^{M,M} = \frac{1}{\hbar\sqrt{|v_{z,<}^{M,j}|\,|v_{z,>}^{M,j'}|}}\left[i(u_>^{M,j'})^\dagger \Gamma_M^{\text{lead}} G_{MM}^r \Gamma_M^{\text{lead}}(u_<^{M,j}) - (u_>^{M,j'})^\dagger \Gamma_M^{\text{lead}}(u_<^{M,j})\right]. \tag{3}$$

where the dependence on $\mathbf{k}_\parallel$ is omitted. The labels M and N denote one of the Ag leads (left or right); the subscripts $>$ and $<$ denote Bloch waves propagating against and towards the junction, respectively; and G_{MN}^r is the submatrix of the retarded Green function of the junctions.

In the Boltzmann equation it is convenient to introduce an auxiliary quantity h to characterize the change of the distribution function f from its equilibrium f_0 with energy,

$$f^j(z, \mathbf{k}_\parallel, E) = f_0(E) - h^j(z, \mathbf{k}_\parallel)\frac{\partial f_0}{\partial E}. \tag{4}$$

The Boltzmann equation for the CPP configuration[38,39] is then

$$\left[v_z^j(\mathbf{k}_\parallel)\frac{\partial}{\partial z} + \frac{1}{\tau}\right] h^j(z, \mathbf{k}_\parallel) - \frac{\mu(z)}{\tau} = -e v_z^j(\mathbf{k}_\parallel)\mathcal{E}_z, \tag{5}$$

where τ is a fictitious relaxation time in the Ag leads (see discussion below); and $\mu(z)$ and $\mathcal{E}_z$ denote the applied electric field and the chemical potential along the z-direction, respectively. A note about the relaxation time τ within the Boltzmann model is in order. Although in a real sample the actual electron relaxation time (whose value we do not know) is always finite in the leads, in our model (and all theoretical considerations of a junction using the Landauer formula) it is assumed that the relaxation time is infinite and the only source of the resistance is the tunnel barrier. On the other hand, the Boltzmann theory can only be applied when there is a finite relaxation time. In practice, we found that for any reasonable value of τ, the calculated four-probe resistance is independent of τ, as one would expect. Therefore the calculation is accurate even with a finite value of τ. We also note that the fictitious lifetime τ does not contribute to the imaginary part of the self-energy, Γ^{lead}, which arises entirely from the coupling between the junction and the leads. The method to solve the Boltzmann equation Eq. (5) numerically is given in the Appendix.

The current density along the z-direction is

$$J = -\frac{e}{2\pi\hbar A}\sum_{\mathbf{k}_\parallel, j}\text{sgn}\left[v_z^j(\mathbf{k}_\parallel)\right] h^j(z, \mathbf{k}_\parallel) \equiv \sum_{\mathbf{k}_\parallel} J_{\mathbf{k}_\parallel}(z), \tag{6}$$

with A the cross section of the unit cell of junction perpendicular to the z-direction. The total current density J is a constant due to the conservation of charge, although each of its components $J_{\mathbf{k}_\parallel}(z)$ is not necessarily a constant. The expression for the local chemical potential (see Appendix B) is $\mu(z) = \left\langle h^j(z, \mathbf{k}_\parallel)\right\rangle_{j,\mathbf{k}_\parallel}$, and the voltage drop across the junction located at $z = z_0$ is equal to $\Delta V = \mu(z_0 + 0^+) - \mu(z_0 - 0^-)$; thus the four-probe resistance of the junction is calculated as $\Delta V/J$.

III. MULTILAYER SILICENE JUNCTIONS

A. Structure and electronic structure

We considered two different stacking orders for the multilayer-silicenes.[5] In the first stacking order, two inequivalent silicene layers are stacked in an "AA" manner (denoted as "AA-Si"), and each Si atom can find another in its neighboring layers with the same in-plane position. The second stacking order, denoted as "ABC-Si", corresponds to the stacking along the (111) direction of diamond-structured silicon. We note that both of these stacking configurations lead to a tetragonal arrangement of Si atoms, as shown in Fig. 2.

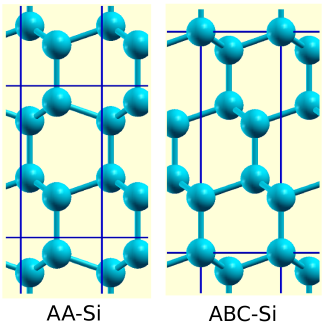

FIG. 2. (Color online) Atomic structures of bulk AA-Si and ABC-Si. The unit cell boundary is denoted by blue lines.

The total energies of bulk AA- and ABC-Si were calculated as a function of the interlayer distance. The interlayer distance is one half (third) of the lattice constant of bulk AA-Si (ABC-Si) along the z-direction. Bulk AA-Si has a higher total energy than bulk ABC-Si by 14 meV per Si atom, as shown in Fig. 3(a).

We also calculated the total energies of multilayer silicene based junctions. The total energies of AA-Si based junctions are always higher than the corresponding ABC-Si junctions, and the total energy difference per Si atom

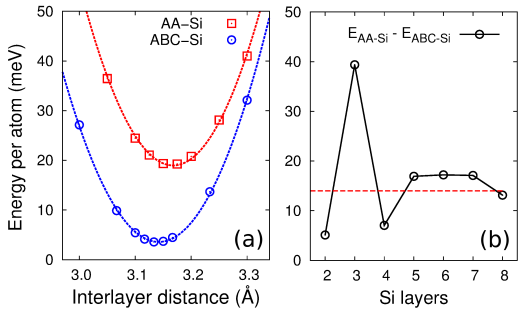

FIG. 3. (Color online) Energetics of (a) bulk AA-Si and ABC-Si, and (b) the energy difference per Si atom between Ag(111)/AA-Si/Ag and Ag(111)/ABC-Si/Ag junctions, as a function of the number of Si layers. The dashed line in (b) shows the difference in the bulk.

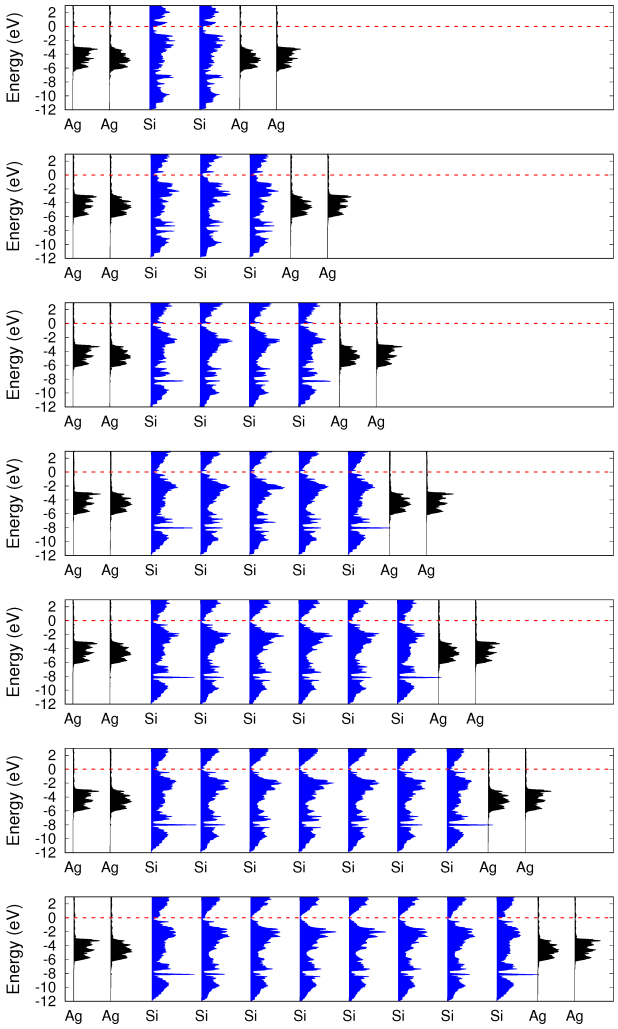

FIG. 4. The projected density of states on each atomic layer in Ag/AA-Si/Ag junctions with the thickness of Si barrier (from top to bottom panel) from 2 to 8 atomic layers. Note that the scale of PDOS on Ag is 15 times larger than Si.

is shown in Fig. 3(b). The energy difference between bulk AA-Si and ABC-Si is denoted as the dashed line in Fig. 3(b). The deviations from the dashed line in Fig. 3(b) are due to interface effects. We have also tried another method to obtain the atomic structures of junctions, in which the junction with $(n+1)$ silicene layers was constructed and optimized from the junction with n silicene layers by inserting a flat Si layer between the nth layer of silicene and the Ag(111) lead. The resulting multilayer silicene structures are different from both AA-Si or ABC-Si, but are similar to the body-centered tetragonal C_4 allotrope of carbon.[52] Results for these structures are not shown due to their much higher energies.

The projected density of states (PDOS) onto each atomic layer of Ag leads and Si barrier is plotted in Fig. 4 for AA-Si and Fig. 5 for ABC-Si junctions respectively, where the PDOS for Ag is scaled by 1/15 relative to that of Si for better visibility. The PDOS near the Fermi

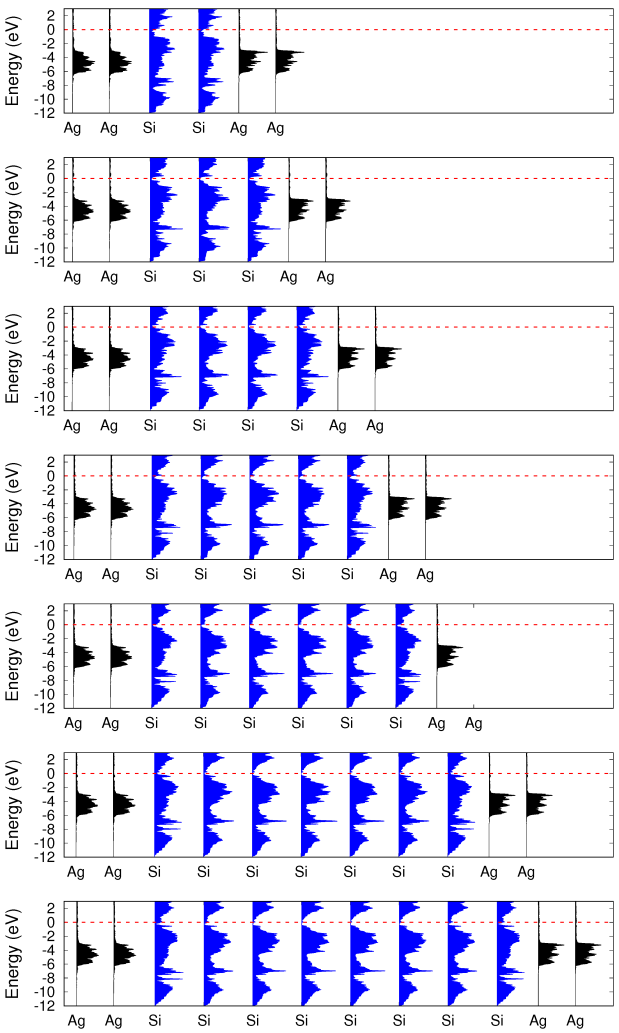

FIG. 5. The projected density of states on each atomic layer in Ag/ABC-Si/Ag junctions with the thickness of Si barrier (from top to bottom panel) from 2 to 8 atomic layers. Note that the scale of PDOS on Ag is 15 times larger than Si.

energy for Ag/Si/Ag junctions with two and eight Si layers is plotted in Fig. 6. The PDOS on Ag is dominated by d-bands between -3 eV and -6 eV, whereas the sp-bands contribute PDOS above -3 eV. The PDOS on Si below the band gap is characterized by three broad peaks centered at -3 eV, -7 eV, and -10 eV, the same as diamond-structure bulk silicon. Deeply buried Si layers in thick-barrier junctions reproduce the density of states of bulk Si. However the Si layers adjacent to Ag leads exhibit different features from bulk Si: i) additional broad peaks emerge between -4 eV and -6 eV due to orbital hybridization with Ag leads, and ii) these Si layers show no energy gaps at the Fermi energy because of the metal-induced gap states, as shown in Fig. 6(a,c). These metal-induced distortions in PDOS are most severe in the first Si atomic layer adjacent to Ag leads, and are also visible in the second Si layer. The PDOS points to a transition from nearly metallic transport to tunneling

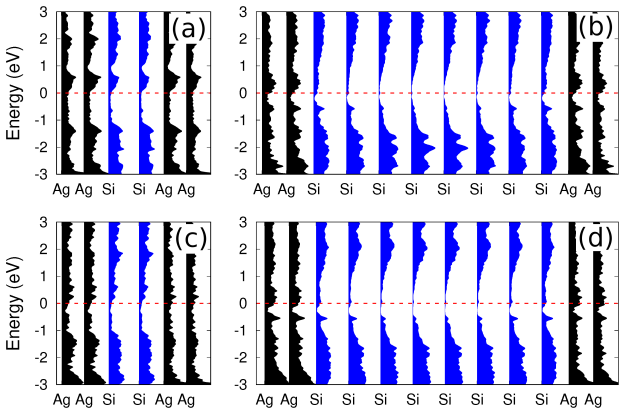

FIG. 6. The projected density of states on each atomic layer near the Fermi energy: Ag/AA-Si/Ag junctions with (a) two and (b) eight Si layers, and Ag/ABC-Si/Ag junctions with (c) two and (d) eight Si layers. The PDOS of Ag is on the same scale with that of Si.

in Ag/Si/Ag junctions as the thickness of Si barrier increases.

B. Transmission

The transmission probabilities of Ag(111)/multilayer-silicene/Ag(111) junctions at the Fermi energy were calculated using the DFT-NEGF method, averaged over $\mathbf{k}_\parallel$-points in the first Brillouin zone,

$$\mathcal{T} = \frac{1}{N_{\mathbf{k}_\parallel}} \sum_{\mathbf{k}_\parallel} T(\mathbf{k}_\parallel). \tag{7}$$

Because there is more than one transverse mode for each $k_\perp$ due to the band structure folding, the averaged transmission $\mathcal{T}$ could be larger than unity. The transmission as a function of Si barrier thickness is shown in Fig. 7 for

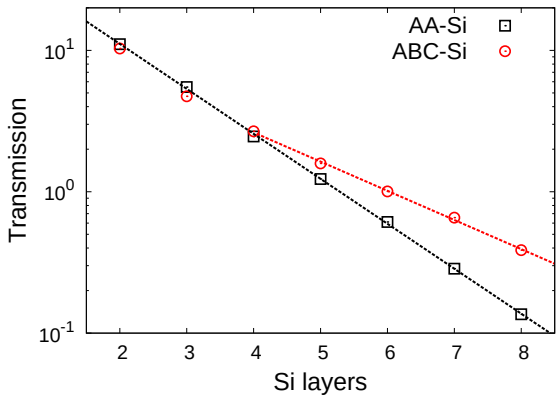

FIG. 7. (Color online) The averaged transmission over $\mathbf{k}_\parallel$ for Ag/AA-Si/Ag and Ag/ABC-Si/Ag junctions as a function of the number of Si layers.

AA- and ABC-Si junctions. For thinner junctions, those with less than four Si layers, the transmissions of AA-Si junctions are very close to those of ABC-Si junctions.

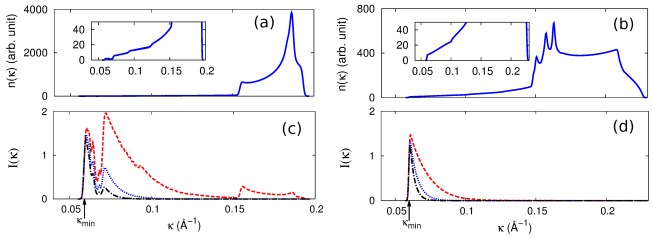

FIG. 8. (Color online) The density of κ, denoted as $n(\kappa)$, for (a) AA-Si and (b) ABC-Si respectively, where κ is defined as $\kappa(\mathbf{k}_\parallel) = \min_{\mathbf{k}_\parallel} \mathrm{Im}(k_z)$; and the relative importance $I(\kappa) = n(\kappa)e^{-\kappa d}/[n(\kappa_{\min})e^{-\kappa_{\min} d}]$ for (c) AA-Si and (d) ABC-Si respectively, with $d = 2$ (dashed, red lines), $d = 4$ (dotted, blue lines), and $d = 6$ (dash-dot, black lines) times of the Si interlayer distance 3.15 Å.

Next we discuss the different transmission decay rates in junctions with thick Si barriers. The tunneling through metal|semiconductor|metal junctions can be understood in terms of the complex band structure of the semiconductor barrier.[53] The tunneling current is carried out by evanescent states near the metal|semiconductor interfaces on the semiconductor side. The energy dispersions of the evanescent and propagating states are called the complex band structure. The junction is assumed to be periodic in the x-y plane, so the in-plane components of the vector $\mathbf{k}_\parallel = (k_x, k_y)$ are always real, while the component along the z-direction k_z is allowed to be complex. The Fermi energy of the junction lies in the band gap region of the semiconductor barrier, so the imaginary part of k_z is always nonzero. Although there are infinitely many k_z for each $\mathbf{k}_\parallel$, we only considered the one with the smallest imaginary part (denoted as κ hereafter), since the corresponding evanescent state has the slowest decay rate.

We calculated κ for each $\mathbf{k}_\parallel$, where all of the $\mathbf{k}_\parallel$'s form a uniform mesh in the two-dimensional first Brillouin zone. Following Ref. 53, the density of κ is defined as $n(\kappa') = \sum_{\mathbf{k}_\parallel} \delta[\kappa(\mathbf{k}_\parallel) - \kappa']$. In practice the δ-function is replaced by a Gaussian function. The calculated densities of κ for AA-Si and for ABC-Si are plotted in Fig. 8(a) and (b), respectively. The density of κ in the high-κ region ($\kappa > 0.15$/Å) is much larger than that in the low-κ region ($\kappa < 0.15$/Å).

Not all of the κ's are important for the tunneling. The relative importance of each evanescent state can be described by a function $I(\kappa)$, defined as[53],

$$I(\kappa) = \frac{n(\kappa)e^{-\kappa d}}{n(\kappa_{\min})e^{-\kappa_{\min} d}}. \quad (8)$$

where d is the thickness of the semiconductor barrier excluding the two interface Si layers which are gapless. In the calculation, the values of d were chosen to correspond to 2, 4, and 6 Si layers for actual Si thicknesses of 4, 6, and 8 layers. The results are plotted in Figs. 8(c) and (d). The values of important κ's of AA-Si, *i.e.* those with a significant $I(\kappa)$, are larger than those of ABC-Si. This explains the faster decay of the transmission in AA-Si based junctions. For very large d the relative importance of all κ except $\kappa_{\min}$ is zero, since $I(\kappa) \propto e^{-2(\kappa-\kappa_{\min})d}$, and the tunneling is contributed only by the evanescent state corresponding to $\kappa_{\min}$. But for thin barriers, κ's larger than $\kappa_{\min}$ can also be important.

C. Resistance

It is well known that the resistance from Landauer-Büttiker formula corresponds to a two-probe measurement[54] with a quantum contact resistance, sometimes equated with the Sharvin resistance, in series with the junction resistance. Experiments employ four-probe measurements where all the contact resistances including the Sharvin resistance are excluded.

There are two widely employed recipes in the literature for calculating the resistance of 3D nano-junctions. The first recipe[55–57] is to directly subtract the semiclassical Sharvin resistance R_{Sharvin} from the result of the Landauer-Büttiker formula. Hereafter this method is referred to as the Sharvin correction method. It is assumed that 1) the geometric contact resistance is equal to the Sharvin resistance and that 2) the geometric contact resistance is in series with the junction resistance. (The second assumption is questionable since Ohm's law is usually violated by interference effects due to phase-coherence.) Controversy also remains for how to calculate the junction resistance arising from elastic scattering.[58] Different assumptions[33–37] on the distribution of current over conducting channels have been proposed, leading to different expressions for the resistance, but there is consensus on three limits. The first is the case of a single conducting channel, where the distribution of current over channels becomes trivial and the resistance is given by the Landauer's formula: $R_{\mathrm{Landauer}} = R_0(1-T)/T$. The second is the small-transmission limit, in which the distinction between different models becomes unimportant; specifically, the spurious contact resistance contained in the Landauer-Büttiker formula becomes negligibly small relative to the junction resistance. The third limit is the obstacle-free limit at zero temperature, in which the resistance caused by elastic scattering is zero, and the geometric contact resistance contained in the Landauer-Büttiker formula reduces to the semiclassical Sharvin resistance. Away from these limiting cases, for 3D nano-junctions with a large transmission probability (on the order of or larger than 0.1) such as grain boundaries in metals[55–57] and the junctions studied in this work, the resistance is severely overestimated by the Landauer-Büttiker formula.

The second recipe[38,39] is to replace the Landauer-Büttiker formula by a hybridized semiclassical-quantum

approach. In this approach the transport of electrons inside the metal leads follows the semiclassical Boltzmann equation in the relaxation-time approximation. The transport across the tunnel barrier is assumed to be phase-coherent and is described using a quantum mechanical theory such as a scattering theory or Green's function method. The voltage drop across the junction is calculated from the local chemical potential in the leads, and the resistance is extracted from the voltage. This method is referred to as the semiclassical Boltzmann (SCB) method; the idea behind this method can be traced to Ref. 58. The method involves the group velocities of electrons, a feature also shared by other theories,[33–37,58] but not by the Landauer-Büttiker/Sharvin recipe in the preceding paragraph.

Both methods yield the expected results in the three limiting cases. Both of the recipes lack a rigorous foundation, so their accuracies can only be ascertained by comparing with experimental results. To our best knowledge, the Σ_3 twin boundaries in copper provide the only system studied by both methods and by experiments. Compared with the experimental resistance,[32] the first recipe[55–57] underestimates the resistance by 7–13% , while the second recipe[29,59,60] overestimates by 19–22% . More work is needed comparing these two methods with each other and with experiments.

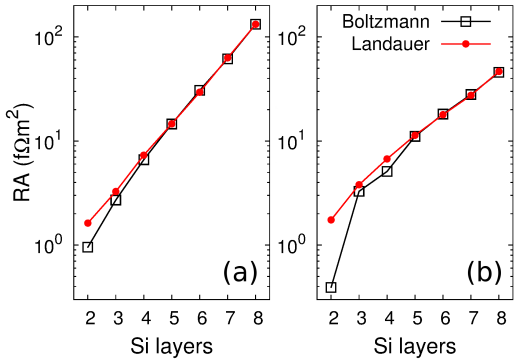

FIG. 9. (Color online) Resistance-area products of (a) Ag/AA-Si/Ag and (b) Ag/ABC-Si/Ag junctions as a function of the number of Si layers calculated using the SCB equation (black squares) and using the Bütikker formula (red dots). Curves for different methods converge for thicker junctions.

Using the Landauer-Büttiker formula, the resistance-area products (RA) of these junctions is

$$\mathrm{RA} = \frac{1}{\mathcal{T}} \frac{2\pi\hbar}{2e^2} A, \tag{9}$$

where $\mathcal{T}$ is the averaged transmission defined in Eq. (7), $2\pi\hbar/2e^2 = 12.9\,\mathrm{k}\Omega$ is the quantum resistance, and A is the cross section of the junction unit cell in the x-y plane. The values of RA calculated using the Landauer-Büttiker formula and using the SCB method as presented in Sec. II are compared in Fig. 9 as a function of the number of Si layers.

We also plot in Fig. 10 the calculated RA's of AA-Si and ABC-Si junctions using the SCB method and using the Landauer-Büttiker formula with and without Sharvin correction[55–57] as a function of transmission per channel. The SCB results are reproduced by the Landauer-Büttiker formula without Sharvin correction in the small transmission region, but difference between the two methods emerge when transmission per channel is larger than 0.05. Although the Sharvin correction to the Landauer-Büttiker formula improves the agreement with the SCB results in the large transmission region, there is still visible difference in the plot. For example, the resistance of the ABC-Si junction with two Si layers (the rightmost circle in Fig. 10) is overestimated by 100% using the Landauer-Büttiker formula with Sharvin correction. This is in contrast with the case of Σ_3 twin boundaries in copper, where the resistance calculated using the SCB method is higher than that using the Landauer-Büttiker formula with Sharvin correction. The Landauer-Büttiker formula gives almost the same RA as the SCB theory for junctions with more than five layers of silicene, where the averaged transmission per channel is about 0.05. In this small transmission limit, the spurious contact resistance implicitly included in the Landauer-Büttiker formula is negligibly small compared to the tunneling resistance. This is the first time that the SCB theory has been applied down to the small transmission region. In this small transmission region, the Boltzmann equation becomes numerically difficult to solve; as a result, it is more convenient to use the Landauer-Büttiker formula instead.

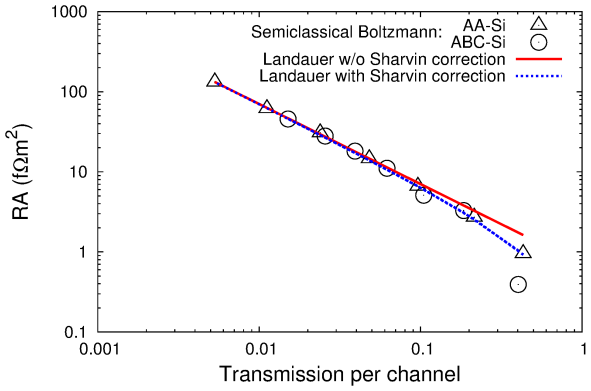

FIG. 10. (Color online) The resistance-area products (RA) as a function of transmission per channel. Curves show RA calculated using the Landauer-Büttiker formula (red solid line) and using the Landauer-Büttiker formula with Sharvin correction (black dotted line). Results using semiclassical Boltzmann equation are shown as symbols: △ for Ag/AA-Si/Ag and ◯ for Ag/ABC-Si/Ag junctions.

The ABC-Si junction with two Si atomic layers has a RA 50% smaller than that of the corresponding AA-Si junction, indicating that the calculated resistance using the SCB theory is not entirely determined by the averaged transmission. The existing various multi-channel

extensions[37,58] of the four-probe Landauer formula have the common feature that the group velocities of Bloch states in the leads play a role. The factors determining the SCB resistance are however rather difficult to analyze, due to the self-consistent nature of the Boltzmann equation. The most important observation from Figs. 9 and 10 is that the upper limit of the transmission per channel for the applicability of the Landauer formula is equal to 0.05. In the next section, we studied *h*-BN-based junctions to explore whether this value (0.05) is universal.

IV. MULTILAYER HEXAGONAL BORON NITRIDE JUNCTIONS

In this section, for comparison and for the interest in layered materials in general we turn to junctions based on the wide-gap insulator hexagonal boron nitride (*h*-BN). Hexagonal boron nitride (*h*-BN), generally recognized as a good insulator because of its large energy band gap, is known to form a nearly perfect interface with nickel (111) direction,[61–66] and has attracted much of current interest because of its ideal interface with graphene.[67–69] However, first-principles calculations in the literature[70,71] showed that the transmission of monolayer *h*-BN-based junctions is on the order of unity. According to the preceding results on multilayer silicene junctions, the Landauer formula is no longer reliable, but instead SCB theory is needed to calculate the resistivity of monolayer *h*-BN junctions.

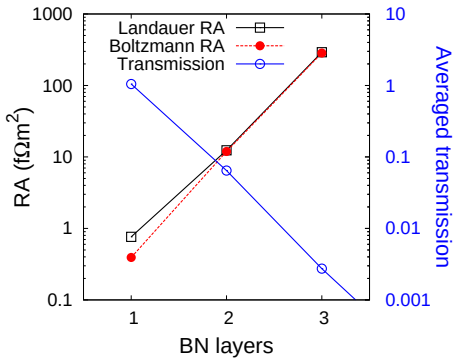

FIG. 11. (Color online) Resistance-area products of Ni(111)|*h*-BN|Ni junctions with different numbers of *h*-BN layers calculated using the Landauer-Büttiker formula (black squares) and using the SCB theory (red dots). The averaged transmission is denoted by blue circles.

The transmissions of mono-, bi-, and tri-layer *h*-BN based junctions are calculated using the same method as for Ag/silicene/Ag junctions, except that spin-polarized calculations were carried out; the magnetic moments in the two Ni(111) leads are set to be parallel to each other. In Fig. 11 The calculated transmission decays exponentially as a function of number of *h*-BN layers, in accord with previous calculations.[71] No spin flip is considered in calculating the resistance, and the two spin channels are considered to be independent. The RA of monolayer *h*-BN-based junctions calculated using the Landauer formula Eq. (9) is about two times larger than that using the SCB theory, as seen in Fig. 11. The difference in RA between the Landauer-Büttiker formula and the SCB theory becomes very small for junctions with more than one *h*-BN layer. The junction with bilayer *h*-BN, the threshold for which the Landauer formula is applicable, again has a transmission of about 0.06, very close to the value 0.05 of the critical transmission for multilayer-silicene junctions.

Different from silicon, *h*-BN is a typical insulator with a large band gap (6.0 eV from experiments[72] and 4.77 eV using DFT[73]). The junction with a monolayer *h*-BN barrier has a surprisingly large transmission and the Landauer-Büttiker formula significantly overestimates its resistance.

V. SUMMARY

In this work we studied the transition from nearly metallic transport to tunneling in Ag/Si/Ag junctions by examining their electronic structure and the transmission probability. In junctions with thin Si barriers, the projected density of states shows no energy gap for Si layers adjacent to Ag leads, and the transmission is independent of the stacking order of the Si layers. For thick junctions, band gap opens for Si layers deeply buried inside thick Si barriers, and the decay rate of the transmission depends on the stacking order of the Si layers.

We calculated the junction resistance using the semiclassical Boltzmann equation method and compared the results to the more often used Sharvin correction method for the Ag/Si/Ag junctions. These calculations show that the Landauer-Büttiker formula works well for transmission values below a critical value of ~ 0.05. This critical value is affirmed by calculations of Ni/*h*-BN/Ni junctions. The fact that these two distinct junctions share the same value of critical transmission (~ 0.05 per channel) proves the universality of this value. This critical value can be employed as a criterion for choosing methods to calculate junction resistance. The Landauer-Büttiker formula is the best choice when the calculated transmission is smaller than this critical value. The SCB theory or the Sharvin correction approach should be used for junctions with larger transmission.

ACKNOWLEDGMENTS

This work was supported by the US Department of Energy (DOE), Office of Basic Energy Sciences (BES), under Contract No. DE-FG02-02ER45995. This research used resources of the National Energy Research Scientific Computing (NERSC) Center.

Appendix A: Numerical solution for the Boltzmann equation

In the appendix the numerical method for solving the Boltzmann equation is presented. The Boltzmann equation in each metallic lead in the CPP geometry is,

$$\left[v_z^j(\mathbf{k}_\parallel)\frac{\partial}{\partial z}+\frac{1}{\tau}\right]h^j(z,\mathbf{k}_\parallel)-\frac{\mu(z)}{\tau}=-ev_z^j(\mathbf{k}_\parallel)\mathcal{E}_z. \tag{A1}$$

The solution of Eq. (A1) can be written as the sum $h^j = u^j + w^j$. The first term u^j satisfies Eq. (A1) for $\mu(z) = 0$,

$$\left[v_z^j(\mathbf{k}_\parallel)\frac{\partial}{\partial z}+\frac{1}{\tau}\right]u^j(z,\mathbf{k}_\parallel)=-ev_z^j(\mathbf{k}_\parallel)\mathcal{E}_z, \tag{A2}$$

for which we can write an analytical solution for u^j,

$$u^j(z,\mathbf{k}_\parallel)=-ev_z^j(\mathbf{k}_\parallel)\mathcal{E}_z\tau+A^j(\mathbf{k}_\parallel)\exp\left[-\frac{z}{v_z^j(\mathbf{k}_\parallel)\tau}\right]; \tag{A3}$$

where the A^j are parameters to be determined by the boundary conditions. Then, w^j obeys

$$v_z^j(\mathbf{k}_\parallel)\frac{\partial w^j(z,\mathbf{k}_\parallel)}{\partial z}+\frac{w^j(z,\mathbf{k}_\parallel)-\mu(z)}{\tau}=0. \tag{A4}$$

Approximating the z dependence of $\mu(z)$ in each metallic lead
to second order,

$$\mu(z)=\mu_0+\mu_1 z+\frac{1}{2}\mu_2 z^2, \tag{A5}$$

we find the solution for w^j is,

$$w^j(z+\Delta z,\mathbf{k}_\parallel)=w^j(z,\mathbf{k}_\parallel)\exp\left[-\frac{\Delta z}{v_z^j(\mathbf{k}_\parallel)\tau}\right]-b_0\mu_0-b_1\mu_1\Delta z-\frac{1}{2}\,b_2\mu_2\Delta z^2, \tag{A6}$$

with

$$b_0=\exp\left[-\frac{\Delta z}{v_z^j(\mathbf{k}_\parallel)\tau}\right]-1, \tag{A7}$$

$$b_1=-\frac{v_z^j(\mathbf{k}_\parallel)\tau}{\Delta z}b_0-1, \tag{A8}$$

$$b_2=-2\frac{v_z^j(\mathbf{k}_\parallel)\tau}{\Delta z}b_1-1. \tag{A9}$$

The z-axis is uniformly discretized in practical calculations. The value of w^j on a grid point can be derived from the value on one of its neighbors, since Eq. (A6) is a recursive type equation.

The boundary conditions for the distribution functions in leads are determined by the transmission and reflection coefficients of the junctions between leads. Here we only considered systems consisting of a single junction sandwiched by two leads; the extension to multiple leads and junctions is straightforward. Suppose the junction between the leads is located at $z = z_0$. The leads above ($z > z_0$) and below ($z < z_0$) the junction are denoted as the "right" (R) and the "left" (L) leads, respectively. The boundary conditions for the distribution function are,

$$h_>^{R,j}(z_0^+)=\sum_{j'}^{N_R}|r_{j,j'}^{RR}|^2\,h_<^{R,j'}(z_0^+)+\sum_{j'}^{N_L}|t_{j,j'}^{LR}|^2\,h_<^{L,j'}(z_0^-) \tag{A10}$$

$$h_>^{L,j}(z_0^-)=\sum_{j'}^{N_L}|r_{j,j'}^{LL}|^2\,h_<^{L,j'}(z_0^-)+\sum_{j'}^{N_R}|t_{j,j'}^{RL}|^2\,h_<^{R,j'}(z_0^+) \tag{A11}$$

The $\mathbf{k}_\parallel$ dependence of the distribution function h and the transmission and reflection coefficients (t and r) are omitted in Eqs. (A10, A11). The total number of channels in the left and the right leads are $2N_L$ and $2N_R$ respectively, half of them propagating towards ($<$) the junction and the other half against ($>$) the junction.

There is a freedom to choose the boundary conditions for v^j and w^j, and in our implementation both v^j and w^j satisfy the boundary conditions Eqs. (A10, A11). Note that since the u^j in Eq. (A3) are decoupled for different $\mathbf{k}_\parallel$'s, so are the boundary conditions in Eqs. (A10, A11). At each $\mathbf{k}_\parallel$, there are $2N_L$ and $2N_R$ unknowns A^j's in the left and right leads respectively, so the total number of unknowns A^j is $2N_L + 2N_R$. The boundary conditions in Eqs. (A10, A11) provide $(N_L + N_R)$ equations, which is less than the number of unknowns by $(N_L + N_R)$. In fact, we considered that the leads have finite lengths, *i.e.*, the left lead extends down to $z = z_L$ and the right lead up to $z = z_R$ ($z_R > z_0 > z_L$). The boundaries at $z = z_L$ and z_R provide boundary conditions similar to Eqs. (A10, A11) but without the transmission part; thus they provide another $N_L + N_R$ equations for determining the unknowns A^j. The reflection coefficients of the boundaries at $z = z_L$ and z_R are arbitrary and they do not change the resistance of the junction if the length of both leads are long enough.

The w^j in Eq. (A4) are no longer decoupled for different $\mathbf{k}_\parallel$, because the chemical potential μ contains a summation over all the $\mathbf{k}_\parallel$'s. As a result, Eq. (A4) for w^j is a self-consistent field equation, which can be solved using an iterative algorithm: given an initial guess for the chemical potential $\mu_{\rm in}(z)$, w^j can be solved using the same method to solve u^j. After solving for $w^j(z)$, a new chemical potential $\mu_{\rm out}(z)$ can be built and used for the next iteration step. The iteration stops when $\mu_{\rm in}(z)$ agrees with $\mu_{\rm out}(z)$ within some predefined numerical accuracy. Efficient mixing algorithms such as given in Ref. 74 can be used to accelerate the convergence. The typical number of iteration steps requried for current-density conservation is several hundreds.

Appendix B: The expression for the local chemical potential

We derive in this Appendix the expression for the local chemical potential $\mu(z)$. The number of electrons at position z with energy E is $\sum_{j,\mathbf{k}_\parallel} f^j(z, \mathbf{k}_\parallel, E)$. The electrons at z are in local equilibrium with a local chemical potential $\mu(\mathbf{r})$, *i.e.*, the occupation number of each mode is equal to $1/(e^{\beta[E-\mu(z)]}+1)$, where $\beta = 1/k_BT$, so we have

$$\sum_{j,\mathbf{k}_\parallel} f^j(z, \mathbf{k}_\parallel, E) = \sum_{j,\mathbf{k}_\parallel} \frac{1}{e^{\beta[E-\mu(z)]}+1}, \tag{B1}$$

or, averaged over j and $\mathbf{k}_\parallel$,

$$\left\langle f^j(z, \mathbf{k}_\parallel, E)\right\rangle_{j,\mathbf{k}_\parallel} = \frac{1}{e^{\beta[E-\mu(z)]}+1} \equiv \mathcal{F}[E-\mu(z)]. \tag{B2}$$

The equilibrium distribution function f_0 denotes electrons that are in global equilibrium with a global chemical potential μ_0,

$$f_0(E) = \mathcal{F}(E-\mu_0). \tag{B3}$$

From Eqs. (B2, B3) in Eq. (4), we have,

$$-\left\langle h^j(z, \mathbf{k}_\parallel)\right\rangle_{j,\mathbf{k}_\parallel} \frac{df_0(E)}{dE} = \mathcal{F}[E-\mu(z)] - \mathcal{F}(E-\mu_0). \tag{B4}$$

In the linear-response regime, the value of $\mu(z)$ remains close to μ_0, and

$$\mathcal{F}[E-\mu(z)] - \mathcal{F}[E-\mu_0] = -[\mu(z)-\mu_0]\left.\frac{d\mathcal{F}(x)}{dx}\right|_{x=E-\mu_0}. \tag{B5}$$

At low temperatures, we have $-df_0(E)/dE = -\left.d\mathcal{F}(x)/dx\right|_{x=E-\mu_0} = \delta(E-\mu_0)$. As a result, the expression for the local chemical potential is

$$\mu(z) = \left\langle h^j(z, \mathbf{k}_\parallel)\right\rangle_{j,\mathbf{k}_\parallel} + \mu_0. \tag{B6}$$

Suppose that $h^j(z, \mathbf{k}_\parallel)$ is the solution of the Boltzmann equation with $\mu(z)$. If the local chemical potential $\mu(z)$ is shifted by a constant C, the corresponding solution of the Boltzmann equation becomes $h^j(z, \mathbf{k}_\parallel) + C$. Both the voltage drop and the current density are independent of the constant C according to their definitions. So, we drop the term μ_0 in the expression of $\mu(z)$ and obtain finally

$$\mu(z) = \left\langle h^j(z, \mathbf{k}_\parallel)\right\rangle_{j,\mathbf{k}_\parallel}. \tag{B7}$$

* Corr. author: Hai-Ping Cheng, hping@ufl.edu

[1] P. De Padova, P. Vogt, A. Resta, J. Avila, I. Razado-Colambo, C. Quaresima, C. Ottaviani, B. Olivieri,

T. Bruhn, T. Hirahara, T. Shirai, S. Hasegawa, M. Carmen Asensio, and G. Le Lay, Appl. Phys. Lett. **102**, 163106 (2013).
[2] P. Vogt, P. Capiod, M. Berthe, A. Resta, P. De Padova, T. Bruhn, G. Le Lay, and B. Grandidier, Appl. Phys. Lett. **104**, 021602 (2014).
[3] P. D. Padova, J. Avila, A. Resta, I. Razado-Colambo, C. Quaresima, C. Ottaviani, B. Olivieri, T. Bruhn, P. Vogt, M. C. Asensio, and G. L. Lay, J. Phys.: Condens. Matter **25**, 382202 (2013).
[4] E. Salomon, R. E. Ajjouri, G. L. Lay, and T. Angot, J. Phys.: Condens. Matter **26**, 185003 (2014).
[5] C. Kamal, A. Chakrabarti, A. Banerjee, and S. K. Deb, J. Phys.: Condens. Matter **25**, 085508 (2013).
[6] Z.-X. Guo and A. Oshiyama, Phys. Rev. B **89**, 155418 (2014).
[7] T. Shirai, T. Shirasawa, T. Hirahara, N. Fukui, T. Takahashi, and S. Hasegawa, Phys. Rev. B **89**, 241403 (2014).
[8] K. Takeda and K. Shiraishi, Phys. Rev. B **50**, 14916 (1994).
[9] E. Durgun, S. Tongay, and S. Ciraci, Phys. Rev. B **72**, 075420 (2005).
[10] G. G. Guzmán-Verri and L. C. Lew Yan Voon, Phys. Rev. B **76**, 075131 (2007).
[11] S. Cahangirov, M. Topsakal, E. Aktürk, H. Şahin, and S. Ciraci, Phys. Rev. Lett. **102**, 236804 (2009).
[12] P. Vogt, P. De Padova, C. Quaresima, J. Avila, E. Frantzeskakis, M. C. Asensio, A. Resta, B. Ealet, and G. Le Lay, Phys. Rev. Lett. **108**, 155501 (2012).
[13] L. Chen, C.-C. Liu, B. Feng, X. He, P. Cheng, Z. Ding, S. Meng, Y. Yao, and K. Wu, Phys. Rev. Lett. **109**, 056804 (2012).
[14] A. Fleurence, R. Friedlein, T. Ozaki, H. Kawai, Y. Wang, and Y. Yamada-Takamura, Phys. Rev. Lett. **108**, 245501 (2012).
[15] L. Meng, Y. Wang, L. Zhang, S. Du, R. Wu, L. Li, Y. Zhang, G. Li, H. Zhou, W. A. Hofer, and H.-J. Gao, Nano Letters **13**, 685 (2013).
[16] C.-L. Lin, R. Arafune, K. Kawahara, M. Kanno, N. Tsukahara, E. Minamitani, Y. Kim, M. Kawai, and N. Takagi, Phys. Rev. Lett. **110**, 076801 (2013).
[17] Z.-X. Guo, S. Furuya, J.-i. Iwata, and A. Oshiyama, Phys. Rev. B **87**, 235435 (2013).
[18] Z.-X. Guo, S. Furuya, J.-i. Iwata, and A. Oshiyama, Journal of the Physical Society of Japan **82**, 063714 (2013).
[19] Y.-P. Wang and H.-P. Cheng, Phys. Rev. B **87**, 245430 (2013).
[20] P. Gori, O. Pulci, F. Ronci, S. Colonna, and F. Bechstedt, J. Appl. Phys. **114**, 113710 (2013).
[21] D. Tsoutsou, E. Xenogiannopoulou, E. Golias, P. Tsipas, and A. Dimoulas, Appl. Phys. Lett. **103**, 231604 (2013).
[22] Y. Wang, Z. Ni, Q. Liu, R. Quhe, J. Zheng, M. Ye, D. Yu, J. Shi, J. Yang, J. Li, and J. Lu, Adv. Funct. Mater. **25**, 68 (2015).
[23] L. Britnell, R. V. Gorbachev, R. Jalil, B. D. Belle, F. Schedin, A. Mishchenko, T. Georgiou, M. I. Katsnelson, L. Eaves, S. V. Morozov, N. M. R. Peres, J. Leist, A. K. Geim, K. S. Novoselov, and L. A. Ponomarenko, Science **335**, 947 (2012).
[24] T. Georgiou, R. Jalil, B. D. Belle, L. Britnell, R. V. Gorbachev, S. V. Morozov, Y.-J. Kim, A. Gholinia, S. J. Haigh, O. Makarovsky, L. Eaves, L. A. Ponomarenko, A. K. Geim, K. S. Novoselov, and A. Mishchenko, Nature Nanotech. **8**, 100 (2013).
[25] L. Britnell, R. M. Ribeiro, A. Eckmann, R. Jalil, B. D. Belle, A. Mishchenko, Y.-J. Kim, R. V. Gorbachev, T. Georgiou, S. V. Morozov, A. N. Grigorenko, A. K. Geim, C. Casiraghi, A. H. C. Neto, and K. S. Novoselov, Science **340**, 1311 (2013).
[26] W. J. Yu, Y. Liu, H. Zhou, A. Yin, Z. Li, Y. Huang, and X. Duan, Nature Nanotechnology **8**, 952 (2013).
[27] D. Sarkar, X. Xie, W. Liu, W. Cao, J. Kang, Y. Gong, S. Kraemer, P. M. Ajayan, and K. Banerjee, Nature **526**, 91 (2015).
[28] H.-M. Li, D. Lee, D. Qu, X. Liu, J. Ryu, A. Seabaugh, and W. J. Yoo, Nature Communications **6**, 6564 (2015).
[29] Y.-P. Wang, J. N. Fry, and H.-P. Cheng, Phys. Rev. B **88**, 125428 (2013).
[30] J. Tersoff, Phys. Rev. B **30**, 4874 (1984).
[31] J. Tersoff, Phys. Rev. B **32**, 6968 (1985).
[32] L. Lu, Y. Shen, X. Chen, L. Qian, and K. Lu, Science **304**, 422 (2004).
[33] P. W. Anderson, D. J. Thouless, E. Abrahams, and D. S. Fisher, Phys. Rev. B **22**, 3519 (1980).
[34] P. W. Anderson, Phys. Rev. B **23**, 4828 (1981).
[35] D. C. Langreth and E. Abrahams, Phys. Rev. B **24**, 2978 (1981).
[36] M. Y. Azbel, J. Phys. C: Solid State Phys. **14**, L225 (1981).
[37] M. D. Ventra, *Electrical Transport in Nanoscale Systems* (Cambridge University Press, 2008).
[38] W. H. Butler, X.-G. Zhang, and J. M. MacLaren, J. Superconduct. **13**, 221 (2000).
[39] W. H. Butler, X.-G. Zhang, and J. M. MacLaren, J. Appl. Phys. **87**, 5173 (2000).
[40] P. E. Blöchl, Phys. Rev. B **50**, 17953 (1994).
[41] G. Kresse and D. Joubert, Phys. Rev. B **59**, 1758 (1999).
[42] G. Kresse and J. Furthmüller, Comput. Mater. Sci. **6**, 15 (1996).
[43] G. Kresse and J. Furthmüller, Phys. Rev. B **54**, 11169 (1996).
[44] J. P. Perdew, K. Burke, and M. Ernzerhof, Phys. Rev. Lett. **77**, 3865 (1996).
[45] E. Rokuta, Y. Hasegawa, K. Suzuki, Y. Gamou, C. Oshima, and A. Nagashima, Phys. Rev. Lett. **79**, 4609 (1997).
[46] S. Datta, *Electronic Transport in Mesoscopic Systems* (Cambridge University Press, Cambridge, 1995).
[47] J. Taylor, H. Guo, and J. Wang, Phys. Rev. B **63**, 245407 (2001).
[48] Y. Xue, S. Datta, and M. A. Ratner, Chem. Phys. **281**, 151 (2002).
[49] M. Brandbyge, J.-L. Mozos, P. Ordejón, J. Taylor, and K. Stokbro, Phys. Rev. B **65**, 165401 (2002).
[50] J. M. Soler, E. Artacho, J. D. Gale, A. Garca, J. Junquera, P. Ordejón, and D. Sánchez-Portal, Journal of Physics: Condensed Matter **14**, 2745 (2002).
[51] N. Troullier and J. L. Martins, Phys. Rev. B **43**, 1993 (1991).
[52] K. Umemoto, R. M. Wentzcovitch, S. Saito, and T. Miyake, Phys. Rev. Lett. **104**, 125504 (2010).
[53] P. Mavropoulos, N. Papanikolaou, and P. H. Dederichs, Phys. Rev. Lett. **85**, 1088 (2000).
[54] X.-G. Zhang and W. H. Butler, Phys. Rev. B **55**, 10308 (1997).
[55] X.-G. Zhang, K. Varga, and S. T. Pantelides, Phys. Rev. B **76**, 035108 (2007).
[56] B.-H. Zhou, Y. Xu, S. Wang, G. Zhou, and K. Xia, Solid State Communications **150**, 1422 (2010).

[57] M. César, D. Liu, D. Gall, and H. Guo, Phys. Rev. Applied **2**, 044007 (2014).
[58] M. Büttiker, Y. Imry, R. Landauer, and S. Pinhas, Phys. Rev. B **31**, 6207 (1985).
[59] T.-H. Kim, X.-G. Zhang, D. M. Micholson, B. M. Evans, N. S. Kulkarni, B. Radhakrishnan, E. A. Kenik, and A.-P. Li, Nano Lett. **10**, 3096 (2010).
[60] M. K. Srivastava, Y. Wang, X.-G. Zhang, D. M. C. Nicholson, and H.-P. Cheng, Phys. Rev. B **86**, 075134 (2012).
[61] C. Oshima and A. Nagashima, Journal of Physics: Condensed Matter **9**, 1 (1997).
[62] W. Auwrter, T. Kreutz, T. Greber, and J. Osterwalder, Surface Science **429**, 229 (1999).
[63] G. B. Grad, P. Blaha, K. Schwarz, W. Auwärter, and T. Greber, Phys. Rev. B **68**, 085404 (2003).
[64] M. Muntwiler, W. Auwrter, F. Baumberger, M. Hoesch, T. Greber, and J. Osterwalder, Surface Science **472**, 125 (2001).
[65] T. Greber, W. Auwärter, M. Hoesch, G. Grad, P. Blaha, and J. Osterwalder, Surface Review and Letters **9**, 1243 (2002).
[66] J. G. Che and H.-P. Cheng, Phys. Rev. B **72**, 115436 (2005).
[67] J. Xue, J. Sanchez-yamagishi, D. Bulmash, P. Jacquod, A. Deshpande, K. Watanabe, T. Taniguchi, P. Jarillo-herrero, and B. J. Leroy, Nature Materials **10**, 282 (2011).
[68] C. R. Dean, A. F. Young, I. Meric, C. Lee, L. Wang, S. Sorgenfrei, K. Watanabe, T. Taniguchi, P. Kim, K. L. Shepard, and J. Hone, Nature Nanotechnology **5**, 722 (2010).
[69] A. K. Geime and I. V. Grigorieva, Nature **499**, 419 (2013).
[70] O. V. Yazyev and A. Pasquarello, Phys. Rev. B **80**, 035408 (2009).
[71] V. M. Karpan, P. A. Khomyakov, G. Giovannetti, A. A. Starikov, and P. J. Kelly, Phys. Rev. B **84**, 153406 (2011).
[72] G. Cassabois, P. Valvin, and B. Gil, Nature Photonics **10**, 262 (2016).
[73] Y.-P. Wang and H.-P. Cheng, Phys. Rev. B **91**, 245307 (2015).
[74] D. D. Johnson, Phys. Rev. B **38**, 12807 (1988).